

# Temporal Brewster anomaly and collimated wave steering in Dirac materials

Seulong Kim<sup>1</sup> and Kihong Kim<sup>2,3\*</sup>

<sup>1</sup>Research Institute of Basic Sciences, Ajou University, Suwon, 16499, Korea.

<sup>2</sup>Department of Physics, Ajou University, Suwon, 16499, Korea.

<sup>3</sup>School of Physics, Korea Institute for Advanced Study, Seoul, 02455, Korea.

\*Corresponding author(s). E-mail(s): [khkim@ajou.ac.kr](mailto:khkim@ajou.ac.kr);

## Abstract

Temporal disorder—random temporal fluctuations of material parameters—has recently emerged as an effective tool for controlling wave propagation, analogous to Anderson localization in spatially disordered systems. Here, we theoretically introduce and analyze the temporal Brewster anomaly in pseudospin-1/2 Dirac systems, demonstrating that Dirac waves remain delocalized along a vector potential with fixed direction despite random temporal variations in its magnitude. In contrast, waves propagating at any off-axis angle exhibit pronounced spatial localization and diffusive behavior. This directional selectivity arises from temporal impedance matching, previously identified as the mechanism suppressing temporal reflection along the vector potential axis. By analyzing temporal reflectance, wave group velocity, and pulse propagation, we establish that these systems function as dynamic directional filters, achieving collimated wave steering purely through temporal modulation. In Dirac materials, external electric fields or mechanical strain can dynamically control the orientation and strength of the vector potential modulation, enabling precise, real-time tuning of directional wave transmission. The temporal Brewster anomaly thus offers a robust and versatile approach for adaptive wave steering, promising significant technological applications in electronic and photonic devices.

**Keywords:** Dirac material, time-varying media, temporal Anderson localization, temporal Brewster anomaly, collimated wave steering, random media

# Introduction

Wave propagation in time-varying media has emerged as a fertile ground for uncovering fundamentally novel physical phenomena [1–8]. A broad range of effects has been explored, including momentum band gaps, temporal aiming, temporal Brewster effects, temporal holography, inverse prisms, antireflection temporal coatings, synthetic axion responses, double-slit time diffraction, and photonic time crystal lasers [9–19]. Substantial research has also been devoted to time-varying dispersive, bianisotropic, and nonlinear media, spatiotemporal modulation, and quantum electrodynamic processes in temporally modulated systems [20–31]. Theoretical advances across these areas have been accompanied by rapid experimental progress [32–38].

Recently, growing attention has turned to temporal disorder—random fluctuations in material parameters over time [39–44]. Such disorder can suppress wave propagation and induce spatial localization, analogous to Anderson localization observed in spatially disordered media [45–47]. While earlier studies predominantly focused on classical electromagnetic waves, recent research has extended these concepts to quantum systems, particularly Dirac-type matter waves [48–52].

In this paper, we introduce and analyze the temporal Brewster anomaly in pseudospin-1/2 Dirac systems, where collimated wave propagation arises solely from temporal modulation. The spatial Brewster anomaly, known from studies of stratified random media, results from specific impedance-matching conditions that enable directional delocalization [53–55]. In earlier work, we derived analogous temporal impedance-matching conditions for Dirac waves and showed that temporal reflection is completely suppressed when the wave vector aligns with a time-dependent vector potential [50]. Furthermore, we demonstrated that random temporal variations generally lead to spatial localization and diffusive wave behavior when such impedance matching is absent [52].

Here, we unify these insights to illustrate a remarkable effect: Dirac waves remain delocalized when propagating parallel to the vector potential direction, despite random temporal modulations. In contrast, off-axis propagation experiences strong spatial localization. Consequently, this system functions as a dynamic directional filter controlled entirely by temporal variations. In electronic Dirac materials, external electric fields provide real-time control over the vector potential via  $\mathbf{E}(t) = -\partial\mathbf{A}(t)/\partial t$ , enabling tunable wave steering [50]. The temporal Brewster anomaly thus presents a versatile mechanism for adaptive wave manipulation, promising significant implications for electronic and photonic technologies.

## Models

We investigate wave dynamics governed by the massless pseudospin-1/2 Dirac equation in a spatially uniform medium under a time-dependent vector potential. In our two-dimensional Dirac model, the vector potential is taken as  $\mathbf{A} = A(t)\hat{\mathbf{x}}$ , aligned along the  $x$ -axis with a time-varying amplitude that can assume both positive and negative values. The wave vector  $\mathbf{k}$  forms an angle  $\theta$  with respect to the  $+x$  direction, making  $\theta$  a key physical parameter in our analysis.

The time-dependent Dirac equation for the two-component wave function  $\Psi = (\psi_1, \psi_2)^T$  is

$$i\hbar \frac{d}{dt} \Psi(t) = \begin{pmatrix} 0 & v_F (\pi_x - i\pi_y) \\ v_F (\pi_x + i\pi_y) & 0 \end{pmatrix} \Psi(t), \quad (1)$$

where

$$\pi_x = \hbar k \cos \theta + eA(t), \quad \pi_y = \hbar k \sin \theta. \quad (2)$$

Here,  $k = |\mathbf{k}|$ ,  $e$  is the electron charge, and  $v_F$  is the Fermi velocity. Since the medium is spatially uniform,  $\mathbf{k}$  is conserved and  $\theta$  remains fixed.

This equation can be recast as a second-order equation for  $\psi_1$ :

$$\frac{d}{dt} \left[ \frac{1}{\epsilon(t)} \frac{d\psi_1}{dt} \right] + \omega_0^2 \epsilon^*(t) \psi_1 = 0, \quad (3)$$

with

$$\epsilon(t) = e^{-i\theta} + \alpha(t), \quad \alpha(t) = \frac{eA(t)}{\hbar k}, \quad \omega_0 = kv_F. \quad (4)$$

The corresponding group velocity is given by

$$\mathbf{v}_g = \pm v_F \left( \frac{\alpha + \cos \theta}{|\epsilon|}, \frac{\sin \theta}{|\epsilon|} \right), \quad (5)$$

where the plus and minus signs refer to particle-like ( $p$ -band) and hole-like ( $h$ -band) states associated with the upper and lower Dirac cones, respectively. Due to the vector potential, the group and phase velocities are generally neither parallel nor antiparallel, except when  $\theta = 0$  or  $\pi$ .

We model the vector potential as

$$\alpha(t) = \alpha_0 + \delta\alpha(t), \quad (6)$$

where  $\alpha_0$  is constant and  $\delta\alpha(t)$  is a random time-dependent fluctuation. Two stochastic models are considered for  $\delta\alpha(t)$ . In Model 1,  $\delta\alpha(t)$  is Gaussian white noise satisfying

$$\langle \delta\alpha(t) \delta\alpha(t') \rangle = g_0 \delta(t - t'), \quad \langle \delta\alpha(t) \rangle = 0, \quad (7)$$

where  $\langle \dots \rangle$  indicates disorder averaging. Using this model and applying the invariant imbedding method with the Furutsu–Novikov formula [52, 56–59], we derive exact differential equations for disorder-averaged quantities. In Model 2,  $\delta\alpha(t)$  takes a constant value over intervals of length  $\tau_d$ , drawn independently from a uniform distribution on  $[-\Delta\alpha, \Delta\alpha]$  and re-randomized at each interval. We study wave propagation by averaging over many realizations and tracking the temporal evolution of wave packets. Since propagation and localization behaviors are expected to be qualitatively robust across different random models, we examine both cases to identify universal features.

## Methods

### Invariant imbedding equations

We consider an incident  $p$ -band wave of unit amplitude, described by  $\psi_1(t) = e^{-i\omega_1 t}$  for  $t \leq 0$ . The spatial dependence of the wave function is given by  $e^{i(k_x x + k_y y)}$  and remains unchanged for all times. When the vector potential varies during the interval  $0 \leq t \leq T$ , the wave function  $\psi_1(t, T)$  takes the form

$$\psi_1(t, T) = \begin{cases} e^{-i\omega_1 t}, & t < 0, \\ r(T)e^{i\omega_2(t-T)} + s(T)e^{-i\omega_2(t-T)}, & t > T, \end{cases} \quad (8)$$

where  $r(T)$  and  $s(T)$  are the temporal reflection and transmission coefficients, respectively. The frequencies  $\omega_i$  ( $i = 1, 2$ ) satisfy

$$\frac{\omega_i}{\omega_0} = |\epsilon_i| \equiv \sqrt{1 + \alpha_i^2 + 2\alpha_i \cos \theta}, \quad (9)$$

with  $\alpha_1$  and  $\alpha_2$  denoting the initial and final values of the normalized vector potential, as defined in Eq. (4).

The coefficients  $r$  and  $s$  correspond to interband ( $p \rightarrow h$ ) and intraband ( $p \rightarrow p$ ) scattering processes, respectively. Using the invariant imbedding method [52, 56, 57], we derive exact differential equations for  $r$  and  $s$  with respect to the imbedding parameter  $\tau$ , representing the duration of the temporal modulation:

$$\frac{1}{\omega_0} \frac{dr}{d\tau} = i\beta r + \gamma s, \quad \frac{1}{\omega_0} \frac{ds}{d\tau} = -\gamma r - i\beta s, \quad (10)$$

where

$$\beta = \frac{1 + \alpha\alpha_2 + (\alpha + \alpha_2) \cos \theta}{|\epsilon_2|}, \quad \gamma = \frac{(\alpha - \alpha_2) \sin \theta}{|\epsilon_2|}. \quad (11)$$

These equations are solved with the initial conditions

$$r(0) = \frac{1}{2} \left( 1 - \frac{\epsilon_2 |\epsilon_1|}{\epsilon_1 |\epsilon_2|} \right), \quad s(0) = \frac{1}{2} \left( 1 + \frac{\epsilon_2 |\epsilon_1|}{\epsilon_1 |\epsilon_2|} \right). \quad (12)$$

The reflectance and transmittance, defined as the ratios of the reflected and transmitted probability densities to that of the incident wave, are given by

$$R = |r|^2, \quad S = |s|^2, \quad (13)$$

with total probability conserved such that

$$R + S = 1 \quad (14)$$

throughout the temporal modulation of  $\alpha(t)$ .

## Moments of the reflection and transmission coefficients

Applying the Furutsu-Novikov formula to Eq. (10) [58, 59], we derive a coupled system of differential equations for the moments  $Z_{abcd} = \langle r^a(r^*)^b s^c(s^*)^d \rangle$ :

$$\begin{aligned} \frac{1}{\omega_0} \frac{d}{d\tau} Z_{abcd} = & C_1 Z_{abcd} + C_2 Z_{a+1,b,c-1,d} \\ & + C_3 Z_{a-1,b,c+1,d} + C_4 Z_{a,b+1,c,d-1} \\ & + C_5 Z_{a,b-1,c,d+1} + C_6 Z_{a+1,b+1,c-1,d-1} \\ & + C_7 Z_{a-1,b-1,c+1,d+1} + C_8 Z_{a+1,b-1,c-1,d+1} \\ & + C_9 Z_{a-1,b+1,c+1,d-1} + C_{10} Z_{a+2,b,c-2,d} \\ & + C_{11} Z_{a-2,b,c+2,d} + C_{12} Z_{a,b+2,c,d-2} \\ & + C_{13} Z_{a,b-2,c,d+2}, \end{aligned} \quad (15)$$

where the coefficients are given by

$$\begin{aligned} C_1 = & i(a-b-c+d)\beta_0 - \frac{g}{2}(a-b-c+d)^2\zeta^2 \\ & - \frac{g}{2}(a+b+c+d+2ac+2bd)\eta^2, \\ C_2 = & -c\gamma_0 - igc(a-b-c+d+1)\zeta\eta, \\ C_3 = & a\gamma_0 + igc(a-b-c+d-1)\zeta\eta, \\ C_4 = & -d\gamma_0 - igd(a-b-c+d-1)\zeta\eta, \\ C_5 = & b\gamma_0 + igb(a-b-c+d+1)\zeta\eta, \\ C_6 = & gcd\eta^2, \quad C_7 = gab\eta^2, \quad C_8 = -gbc\eta^2, \quad C_9 = -gad\eta^2, \\ C_{10} = & \frac{g}{2}c(c-1)\eta^2, \quad C_{11} = \frac{g}{2}a(a-1)\eta^2, \\ C_{12} = & \frac{g}{2}d(d-1)\eta^2, \quad C_{13} = \frac{g}{2}b(b-1)\eta^2. \end{aligned} \quad (16)$$

The parameters are defined as

$$\begin{aligned} \beta_0 = & \frac{1 + \alpha_0\alpha_2 + (\alpha_0 + \alpha_2)\cos\theta}{|\epsilon_2|}, \quad \gamma_0 = \frac{(\alpha_0 - \alpha_2)\sin\theta}{|\epsilon_2|}, \\ \zeta = & \frac{\alpha_2 + \cos\theta}{|\epsilon_2|}, \quad \eta = \frac{\sin\theta}{|\epsilon_2|}, \quad g = g_0\omega_0. \end{aligned} \quad (17)$$

The initial conditions are given by  $Z_{abcd}(0) = [r(0)]^a[r^*(0)]^b[s(0)]^c[s^*(0)]^d$ . In particular, when the vector potentials before and after the modulation are equal (i.e.,  $\alpha_1 = \alpha_2$ ), the initial conditions reduce to  $Z_{abcd}(0) = 1$  if  $a = b = 0$ , and  $Z_{abcd}(0) = 0$  otherwise.

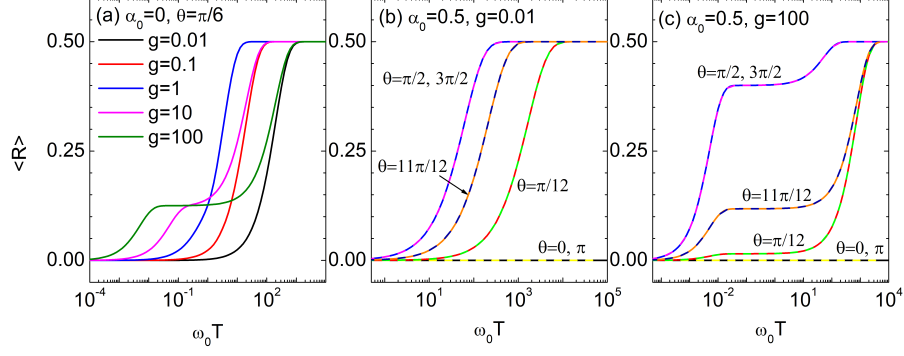


**Fig. 1** Time evolution of disorder-averaged reflectance. (a) Reflectance for various disorder strengths  $g$  at fixed  $\alpha_0 = 0$  and  $\theta = \pi/6$ ; (b) Reflectance for various  $\theta$  under weak disorder ( $g = 0.01$ ) with  $\alpha_0 = 0.5$ ; (c) Reflectance for various  $\theta$  under strong disorder ( $g = 100$ ) with  $\alpha_0 = 0.5$ . Solid lines represent numerical results obtained by solving Eq. (15); dashed lines indicate analytical solutions from Eq. (18) in (b) and Eq. (19) in (c).

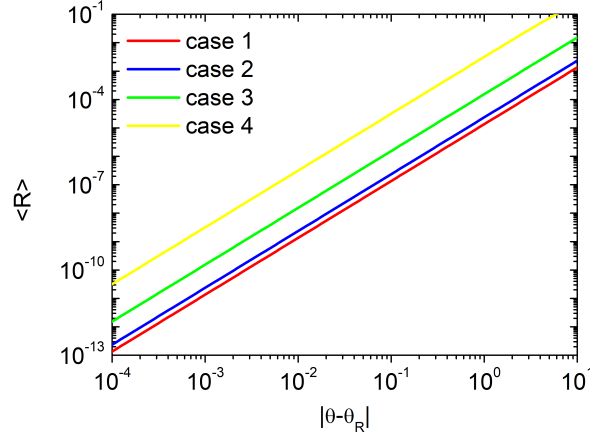


**Fig. 2** Quadratic dependence of disorder-averaged reflectance near  $\theta = \theta_R$  (0 or  $\pi$ ). Disorder-averaged reflectance as a function of  $\theta - \theta_R$  is shown for four representative parameter sets: (1)  $g = 0.01$ ,  $\alpha_0 = 0.5$ ,  $\omega_0 T = 10$ ,  $\theta_R = 0$ ; (2)  $g = 0.1$ ,  $\alpha_0 = 0.1$ ,  $\omega_0 T = 1$ ,  $\theta_R = 0$ ; (3)  $g = 1$ ,  $\alpha_0 = 0.2$ ,  $\omega_0 T = 0.5$ ,  $\theta_R = \pi$ ; (4)  $g = 10$ ,  $\alpha_0 = 0$ ,  $\omega_0 T = 100$ ,  $\theta_R = \pi$ . In all cases, the reflectance exhibits a universal quadratic scaling,  $\langle R \rangle \propto (\theta - \theta_R)^2$ , near  $\theta_R$ .

## Results

We begin by analyzing the temporal evolution of the average reflectance,  $\langle R \rangle$ , obtained by solving Eq. (15), which remains valid for arbitrary disorder strength  $g$ . For simplicity, we consider the case where the vector potentials before and after the interval, as well as the average value during it, are identical; that is,  $\alpha_1 = \alpha_2 = \alpha_0$ . When  $\theta = 0$  or  $\pi$ , we have  $\gamma_0 = \eta = 0$ , and Eq. (15) yields  $\langle R \rangle = 0$  and  $\langle S \rangle = 1$ , indicating perfect transmission regardless of temporal variation in  $A$ .

For general  $\theta$ , analytical expressions can be derived in both the weak and strong disorder limits. In the weak disorder regime, we find

$$\langle R \rangle = \frac{1}{2} \left[ 1 - \exp \left( -\frac{2g\omega_0 \sin^2 \theta}{|\epsilon_0|^2} t \right) \right], \quad (18)$$

where  $|\epsilon_0| = \sqrt{1 + \alpha_0^2 + 2\alpha_0 \cos \theta}$ . In the strong disorder regime, numerical analysis yields

$$\langle R \rangle = \frac{1}{2} (1 - e^{-2g\omega_0 t}) \left[ 1 - \left( 1 - \frac{\sin^2 \theta}{|\epsilon_0|^2} \right) \exp \left( -\frac{2\omega_0 \sin^2 \theta}{g} t \right) \right]. \quad (19)$$

In both limits, for any  $\theta \neq 0$  or  $\pi$ , the average reflectance approaches  $1/2$  exponentially in the long-time limit.

In Fig. 1, we show the time evolution of  $\langle R \rangle$  under various conditions. In Fig. 1(a), the angle is fixed at  $\theta = \pi/6$  and the average vector potential is set to  $\alpha_0 = 0$ , while the disorder strength  $g$  is varied. In Figs. 1(b) and 1(c),  $\alpha_0$  is fixed at  $0.5$ , and the reflectance is plotted for several values of  $\theta$  under weak ( $g = 0.01$ ) and strong ( $g = 100$ ) disorder, respectively. In all cases, the reflectance begins at zero, increases exponentially, and eventually saturates at  $1/2$ , except at  $\theta = 0$  or  $\pi$ , where it remains zero due to perfect transmission. In the weak disorder regime, the approach to saturation becomes faster with increasing  $g$ , while in the strong disorder regime, it slows down.

Near  $\theta_R = 0$  or  $\pi$ , the average reflectance  $\langle R \rangle$  exhibits a universal quadratic dependence on  $\theta - \theta_R$ , regardless of the disorder strength, average vector potential, or modulation duration. Figure 2 demonstrates this scaling for four representative cases: weak disorder in the intermediate-time regime, moderate and strong disorder in the short-time regime, and very strong disorder in the long-time regime. In all cases,  $\langle R \rangle \propto (\theta - \theta_R)^2$  when  $|\theta - \theta_R|$  is sufficiently small.

From the identity  $S + R = 1$ , it follows that for  $\theta \neq 0, \pi$ , the difference  $\langle S - R \rangle = 1 - 2\langle R \rangle$  characterizes the net wave propagation. This quantity is proportional to both the electrical current density and the average group velocity [52]. In the weak disorder regime, Eq. (18) gives

$$\langle S - R \rangle = e^{-t/\tau_w}, \quad \tau_w = \frac{1 + \alpha_0^2 + 2\alpha_0 \cos \theta}{2g\omega_0 \sin^2 \theta}. \quad (20)$$

In the strong disorder regime, for sufficiently large  $t$ , the decay is governed by

$$\langle S - R \rangle \propto e^{-t/\tau_s}, \quad \tau_s = \frac{g}{2\omega_0 \sin^2 \theta}. \quad (21)$$

Using  $g = g_0\omega_0 = g_0kv_F$ , we find that  $\tau_w \propto g_0^{-1}k^{-2}$ , while  $\tau_s \propto g_0$  and is independent of  $k$ . Both decay times scale as  $\sin^{-2} \theta$ , indicating that the net current vanishes asymptotically unless  $\theta = 0$  or  $\pi$ . In the weak disorder regime, the net current decays faster

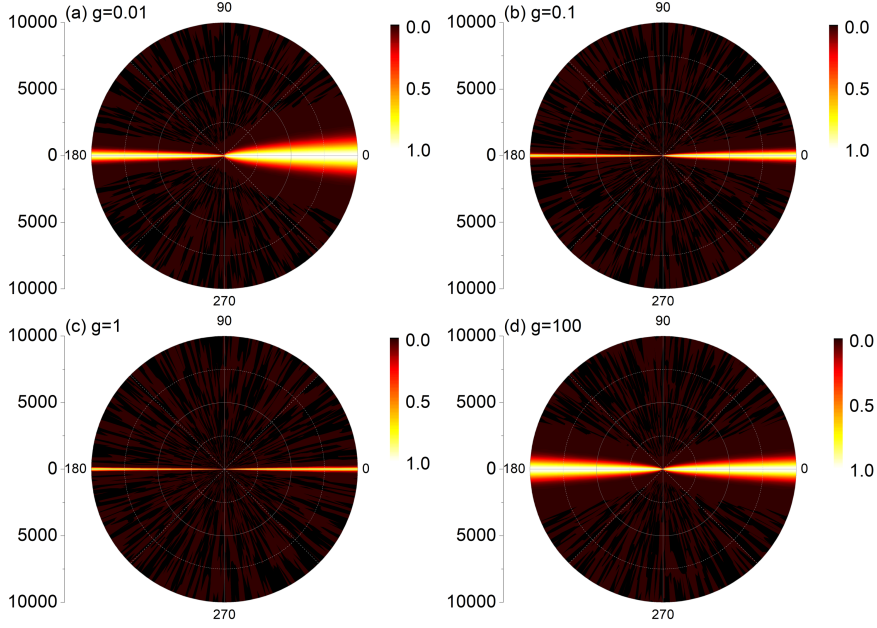


**Fig. 3** Polar plots of the net current  $\langle S - R \rangle$  for varying disorder strengths. Time evolution of  $\langle S - R \rangle$  is shown in polar coordinates for (a)  $g = 0.01$ , (b)  $g = 0.1$ , (c)  $g = 1$ , and (d)  $g = 100$ , with fixed  $\alpha_0 = 0.5$ . The radial coordinate represents time, and the angular coordinate corresponds to  $\theta$ .

with increasing  $g$ . In the strong disorder regime, the decay proceeds in two stages:  $\langle S - R \rangle$  initially drops rapidly from 1 to  $1 - \sin^2 \theta / |\epsilon_0|^2$  on a timescale  $\sim (2g\omega_0)^{-1}$ , followed by a slower decay to zero, with the final-stage timescale increasing with  $g$ . Thus, stronger disorder slows the asymptotic decay of the net current.

In Fig. 3, we show the time evolution of  $\langle S - R \rangle$  in polar coordinates for various disorder strengths  $g$ , with the average vector potential fixed at  $\alpha_0 = 0.5$ . The radial coordinate represents time and the angular coordinate corresponds to the angle  $\theta$  between the vector potential and the wave vector. A finite value of  $\langle S - R \rangle$  indicates net wave propagation in that direction, while values near zero signify effective cessation of propagation. Over time,  $\langle S - R \rangle$  decays exponentially from 1 to 0 for all  $\theta$  except in narrow regions near  $\theta = 0$  and  $\pi$ , where transmission persists—this is a manifestation of the temporal Brewster anomaly. In the weak disorder regime, the angular window supporting propagation narrows with increasing  $g$ , whereas in the strong disorder regime, it broadens as  $g$  increases further. Additionally, in the weak disorder regime, the decay rate depends asymmetrically on  $\alpha_0$  and  $\theta$  [see Eq. (20)], leading to directional asymmetry between  $\theta = 0$  and  $\pi$ . This asymmetry vanishes in the strong disorder limit.

We now analyze wave propagation in Model 2. Although the specific form of randomness differs from that in Model 1, the qualitative features of wave localization remain unchanged, with only quantitative variations. In Fig. 4(a), we show the time evolution of the net current  $\langle S - R \rangle$  for various values of  $\theta$ , with parameters  $\Delta\alpha = 1$ ,  $\alpha_0 = 0$ , and  $\omega_0\tau_d = 10$ , averaged over  $10^6$  random realizations. For  $\theta = 0$ , no temporal



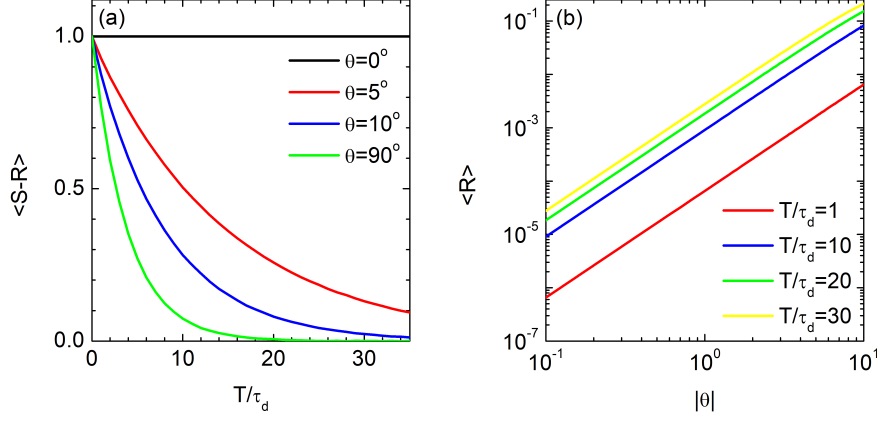


**Fig. 4** Directional wave localization and reflectance behavior in Model 2. (a) Time evolution of the net current  $\langle S - R \rangle$  for various values of  $\theta$ , averaged over  $10^6$  realizations with  $\Delta\alpha = 1$ ,  $\alpha_0 = 0$ , and  $\omega_0\tau_d = 10$ . The net current remains constant at 1 for  $\theta = 0$ , while it decays exponentially over time for  $\theta \neq 0$ . (b) Disorder-averaged reflectance as a function of  $|\theta|$  for different durations of temporal variation. In all cases,  $\langle R \rangle$  exhibits a quadratic dependence on  $\theta$  in the small-angle regime.

scattering occurs, and the net current remains constant at 1. In contrast, for  $\theta \neq 0$ ,  $\langle S - R \rangle$  decays exponentially, signaling the suppression of forward propagation due to temporal Anderson localization. In Fig. 4(b), we plot the disorder-averaged reflectance as a function of  $|\theta|$  for various modulation durations. As in Model 1, the reflectance exhibits a quadratic dependence near  $\theta = 0$ , following  $\langle R \rangle \propto \theta^2$ .

These results confirm the emergence of a temporal Brewster anomaly for Dirac-type waves and particles subjected to random time-dependent vector potentials. Spatial localization occurs for all  $\theta \neq 0, \pi$ , irrespective of the specific form of disorder, while delocalization persists at  $\theta = 0$  and  $\pi$ . Using Model 2, we further demonstrate that wave packets propagate exclusively along these special directions.

We consider a two-dimensional pulse initially centered at the origin with a Gaussian momentum profile:

$$u(x, y, t) = \int_{-\infty}^{\infty} \int_{-\infty}^{\infty} D(k_x, k_y) e^{ik_x x + ik_y y} \Psi(k_x, k_y, t) dk_x dk_y, \quad (22)$$

where  $\Psi(k_x, k_y, t)$  for  $t > T$  and  $D(k_x, k_y)$  are given by

$$\begin{aligned} \Psi(k_x, k_y, t) = & s(k_x, k_y, T) \left( \frac{1}{\epsilon_2^*(k_x, k_y) / |\epsilon_2(k_x, k_y)|} \right) e^{-i\omega_2(t-T)} \\ & + r(k_x, k_y, T) \left( \frac{1}{-\epsilon_2^*(k_x, k_y) / |\epsilon_2(k_x, k_y)|} \right) e^{i\omega_2(t-T)}, \\ D(k_x, k_y) = & e^{-\frac{k_x^2 + k_y^2}{2\sigma_k^2}}, \quad \omega_2 = |\epsilon_2| k v_F. \end{aligned} \quad (23)$$

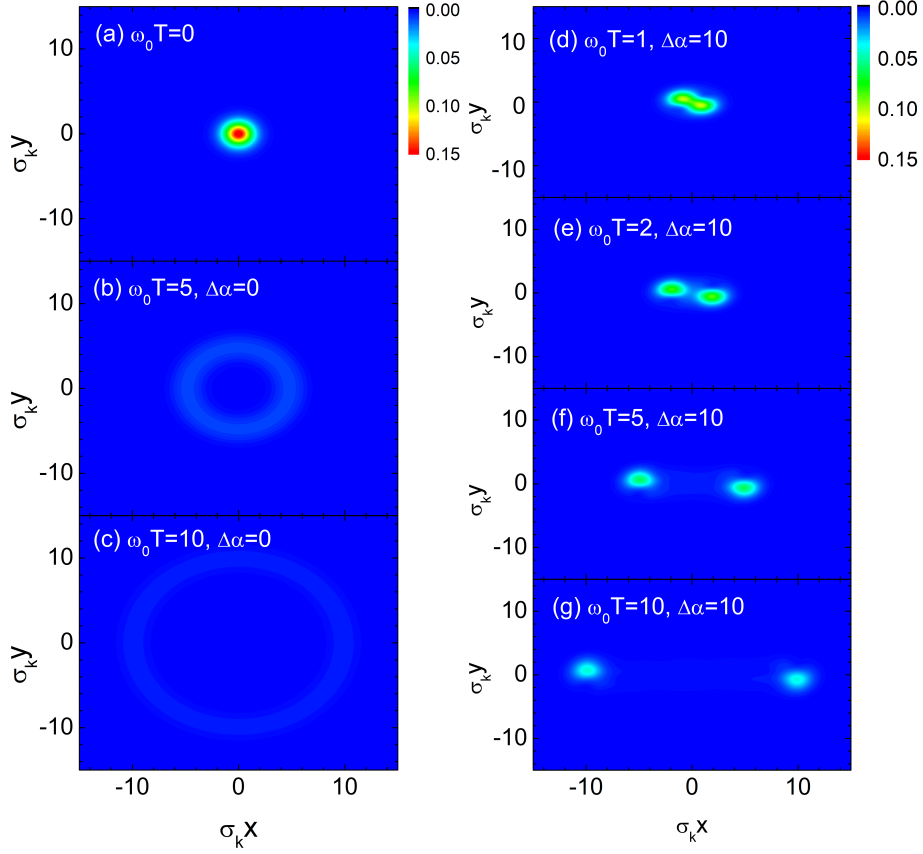


**Fig. 5** Temporal evolution of a two-dimensional pulse in stationary and time-disordered media. (a–c) In a stationary medium, the pulse spreads isotropically, expanding outward in all directions. (a, d–g) When the vector potential varies randomly over time along the  $x$ -axis with strength  $\Delta\alpha = 10$ , the Dirac wave becomes spatially localized and propagates only along the  $\pm x$  directions, causing the pulse to split into two lobes. Results are averaged over 200 random realizations, with  $\sigma_k \tau_d = 1$ .

Here,  $\epsilon_2$  is set to the value of  $\epsilon$  at the final time step corresponding to the given duration  $T$ . The normalized field intensity  $F(x, y, T)$  is obtained from

$$F(x, y, T) = \frac{|u(x, y, T)|^2}{\int_{-\infty}^{\infty} \int_{-\infty}^{\infty} |u(x, y, 0)|^2 dx dy}. \quad (24)$$

In Fig. 5, we illustrate the temporal evolution of a two-dimensional pulse originating from the origin, composed of wave vectors with an isotropic Gaussian profile. In a stationary medium, the pulse expands uniformly in all directions, forming a circular front whose amplitude gradually diminishes due to spatial spreading. In contrast, when the magnitude of the vector potential varies randomly in time with strength

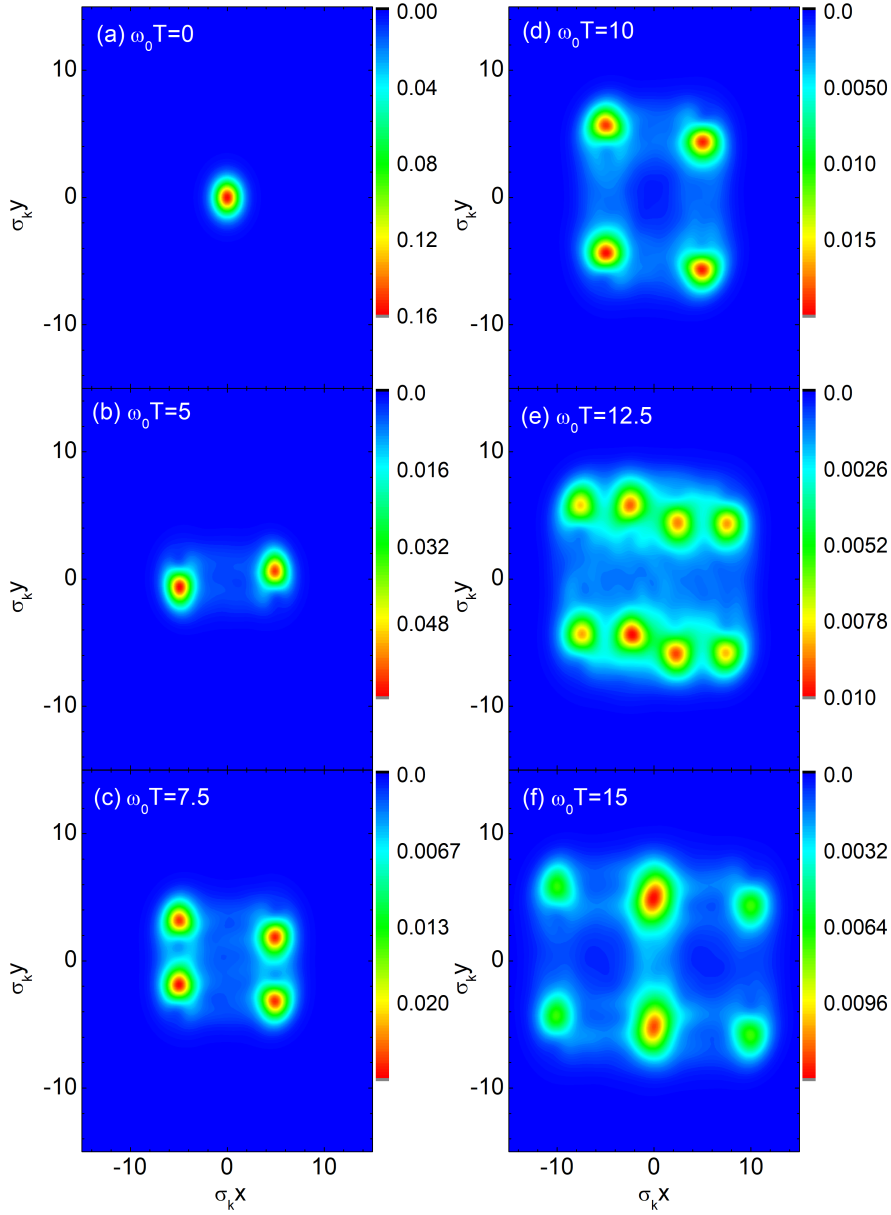


**Fig. 6** Steering of a Dirac pulse via directional modulation of a time-disordered vector potential. A Dirac pulse propagates in a medium where the direction of the temporally disordered vector potential alternates between the  $x$ - and  $y$ -axes every  $\omega_0 T = 5$ . The disorder strength is  $\Delta\alpha = 10$ , and results are averaged over 200 random realizations with  $\sigma_k \tau_d = 1$ . (a) A Gaussian pulse is initially at the origin. (b) For  $0 < \omega_0 T < 5$ , the vector potential points along the  $x$ -axis, steering the pulse along  $\pm x$  and forming two lobes. (c,d) For  $5 < \omega_0 T < 10$ , switching to the  $y$ -axis redirects the pulse along  $\pm y$ , producing four lobes. (e) For  $10 < \omega_0 T < 15$ , the direction returns to the  $x$ -axis, further splitting the wave into eight lobes. (f) At  $\omega_0 T = 15$ , interference near  $x = 0$  leads to partial merging, resulting in six distinct lobes.

$\Delta\alpha = 10$ , while its direction is fixed along the  $x$ -axis, the Dirac wave becomes spatially localized and cannot propagate except along  $\theta = 0$  or  $\pi$ . Consequently, the pulse splits into two components that travel exclusively along the  $\pm x$  directions. This highly directional behavior is a real-space manifestation of the temporal Brewster anomaly. Although the amplitude still decays over time, confinement to two directions significantly slows the decay, allowing the pulse to retain a relatively high amplitude over an extended duration.

Finally, we demonstrate that the direction of wave propagation can be dynamically controlled in real time. In Fig. 6, we show the evolution of a pulse under a time-varying vector potential whose direction alternates between the  $x$ - and  $y$ -axes every  $\omega_0 T = 5$ . The disorder strength is fixed at  $\Delta\alpha = 10$ , and the results are averaged over 200 random realizations with  $\sigma_k \tau_d = 1$ . During the first interval ( $0 < \omega_0 T < 5$ ), the vector potential points along the  $x$ -axis, inducing wave steering along  $\pm x$  and splitting the pulse into two lobes. In the second interval ( $5 < \omega_0 T < 10$ ), the direction switches to the  $y$ -axis, leading to steering along  $\pm y$  and producing four lobes. In the third interval ( $10 < \omega_0 T < 15$ ), the vector potential returns to the  $x$ -axis, causing further splitting into eight lobes. At  $\omega_0 T = 15$ , interference near  $x = 0$  results in partial merging, yielding six distinct lobes. These results highlight how modulation of the vector potential direction enables dynamic wave steering and real-time control of transport pathways via the temporal Brewster effect.

## Discussion

The phenomena uncovered in this study can be experimentally investigated in Dirac materials such as graphene, where an in-plane electric field provides the required time-dependent vector potential [60]. This setup is expected to produce highly directional filtering of electrical currents. A similar effect can also be explored using electromagnetic waves in metamaterials with Dirac-type dispersion, where externally applied strain can serve as an effective vector potential [61, 62].

Taking  $v_F \sim 10^6$  m/s and an electron energy of about 0.1 eV [63–65], the wavenumber is estimated as  $k \sim 1.5 \times 10^8$  m<sup>-1</sup>. For the condition  $\Delta\alpha = 1$ , we find  $\Delta A \sim 1 \times 10^{-7}$  V·s/m. Given  $\omega_0 \tau_D = 10$ , dividing  $\Delta A$  by  $\tau_D$  results in an electric field of approximately  $1.5 \times 10^{-4}$  V/Å, well within the capabilities of current high-power femtosecond laser systems. Thus, the proposed modulation scheme is experimentally feasible.

These findings provide new avenues for wave manipulation in time-dependent media, significantly impacting solid-state physics, optics, and photonic device engineering. The temporal Brewster anomaly, in particular, could inspire innovative optical components, including directional temporal waveguides and dynamic wave filters with spatial focusing and selective transmission capabilities.

Applying similar concepts to classical waves, such as electromagnetic or acoustic waves, holds limited interest due to their exponential amplification under random temporal modulations despite spatial localization of pulses [39–41]. However, by managing exponential energy growth through tailored temporal boundary conditions [66], analogous phenomena can occur, enabling intriguing applications.

## Acknowledgments

This research was supported by the Basic Science Research Program through the National Research Foundation of Korea funded by the Ministry of Education (NRF-2021R1A6A1A10044950).

## References

- [1] Morgenthaler, F. R. Velocity modulation of electromagnetic waves. *IRE Trans. Microwave Theory Tech.* **6**, 167–172 (1958).
- [2] Felsen, L. B. & Whitman, G. M. Wave propagation in time-varying media. *IEEE Trans. Antennas Propag.* **18**, 242–253 (1970).
- [3] Shvartsburg, A. B. Optics of nonstationary media. *Phys.-Uspekhi* **48**, 797–823 (2005).
- [4] Kalluri, D. K. *Electromagnetics of Time Varying Complex Media: Frequency and Polarization Transformer* (CRC Press, Boca Raton, 2010).
- [5] Sounas, D. L. & Alù, A. Non-reciprocal photonics based on time modulation. *Nat. Photonics* **11**, 774–783 (2017).
- [6] Galiffi *et al.* Photonics of time-varying media. *Adv. Photonics* **4**, 014002 (2022).
- [7] Mostafa, M. H., Mirmoosa, M. S., Sidorenko, M. S., Asadchy, V. S. & Tretyakov, S. A. Temporal interfaces in complex electromagnetic materials: an overview. *Opt. Mater. Express* **14**, 1103–1127 (2024).
- [8] Asgari, M. M. *et al.* Theory and applications of photonic time crystals: a tutorial. *Adv. Opt. Photonics* **16**, 958–1063 (2024).
- [9] Zurita-Sánchez, J. R., Halevi, P. & Cervantes-González, J. C. Reflection and transmission of a wave incident on a slab with a time-periodic dielectric function  $\epsilon(t)$ . *Phys. Rev. A* **79**, 053821 (2009).
- [10] Lustig, E., Sharabi, Y. & Segev, M. Topological aspects of photonic time crystals. *Optica* **5**, 1390–1395 (2018).
- [11] Koutserimpas, T. T. & Fleury, R. Electromagnetic waves in a time periodic medium with step-varying refractive index. *IEEE Trans. Antennas Propag.* **66**, 5300–5307 (2018).
- [12] Pacheco-Peña, V. & Engheta, N. Temporal aiming. *Light Sci. Appl.* **9**, 129 (2020).
- [13] Pacheco-Peña, V. & Engheta, N. Temporal equivalent of the Brewster angle. *Phys. Rev. B* **104**, 214308 (2021).

- [14] Bacot, V., Labousse, M., Eddi, A., Fink, M. & Fort, E. Time reversal and holography with spacetime transformations. *Nat. Phys.* **12**, 972–977 (2016).
- [15] Akbarzadeh, A., Chamanara, N. & Caloz, C. Inverse prism based on temporal discontinuity and spatial dispersion. *Opt. Lett.* **43**, 3297–3300 (2018).
- [16] Pacheco-Peña, V. & Engheta, N. Antireflection temporal coatings. *Optica* **7**, 323–331 (2020).
- [17] Prudêncio, F. R. & Silveirinha, M. G. Synthetic axion response with space-time crystals. *Phys. Rev. Appl.* **19**, 024031 (2023).
- [18] Tirole, R. *et al.* Double-slit time diffraction at optical frequencies. *Nat. Phys.* **19**, 999–1002 (2023).
- [19] Lyubarov, M. *et al.* Amplified emission and lasing in photonic time crystals. *Science* **377** 425–428 (2022).
- [20] Solis, D. M., Kastner, R. & Engheta, N. Time-varying materials in the presence of dispersion: plane-wave propagation in a Lorentzian medium with temporal discontinuity. *Photonics Res.* **9**, 091842 (2021).
- [21] Horsley, S. A. R., Galiffi, E. & Wang, Y.-T. Eigenpulses of dispersive time-varying media. *Phys. Rev. Lett.* **130**, 203803 (2023).
- [22] Koutserimpas T. T. & Monticone, F. Time-varying media, dispersion, and the principle of causality. *Opt. Mater. Express* **14**, 1222–1236 (2024).
- [23] Rizza, C. *et al.* Harnessing the natural resonances of time-varying dispersive interfaces. *Phys. Rev. Lett.* **133**, 186902 (2024).
- [24] Koufidis, S. F., Koutserimpas, T. T., Monticone, F. & McCall, M. W. Electromagnetic wave propagation in time-periodic chiral media. *Opt. Mater. Express* **14**, 3006–3029 (2024).
- [25] Mirmoosa, M. S., Mostafa, M. H., Norrman, A. & Tretyakov, S. A. Time interfaces in bianisotropic media. *Phys. Rev. Res.* **6**, 1842–1853 (2024).
- [26] Pan, Y., Cohen, M.-I. & Segev, M. Superluminal  $k$ -gap solitons in nonlinear photonic time crystals. *Phys. Rev. Lett.* **130**, 233801 (2023).
- [27] Tirole, R. *et al.* Second harmonic generation at a time-varying interface. *Nat. Commun.* **15**, 7752 (2024).
- [28] Konforty, N. *et al.* Second harmonic generation and nonlinear frequency conversion in photonic time-crystals. *Light Sci. Appl.* **14**, 152 (2025).

- [29] Galiffi, E., Huidobro, P. A. & Pendry, J. B. Broadband nonreciprocal amplification in luminal metamaterials. *Phys. Rev. Lett.* **123**, 206101 (2019).
- [30] Horsley, S. A. R. & Pendry, J. B. Quantum electrodynamics of time-varying gratings. *Proc. Natl. Acad. Sci. U.S.A.* **120**, e2302652120 (2023).
- [31] Pendry, J. B. & Horsley, S. A. R. QED in space-time varying materials. *APL Quantum* **1**, 020901 (2024).
- [32] Zhou, Y. *et al.* Broadband frequency translation through time refraction in an epsilon-near-zero material. *Nat. Commun.* **11**, 2180 (2020).
- [33] Miyamaru, F. *et al.* Ultrafast frequency-shift dynamics at temporal boundary induced by structural-dispersion switching of waveguides. *Phys. Rev. Lett.* **127**, 053902 (2021).
- [34] Moussa, H. *et al.* Observation of temporal reflection and broadband frequency translation at photonic time interfaces. *Nat. Phys.* **19**, 863–868 (2023).
- [35] Lustig, E. *et al.* Time-refraction optics with single cycle modulation. *Nanophotonics* **12**, 2221–2230 (2023).
- [36] Dong, Z. *et al.* Quantum time reflection and refraction of ultracold atoms. *Nat. Photonics* **18**, 68–73 (2024).
- [37] Jones, T. R., Kildishev, A. V., Segev, M. & Peroulis, D. Time-reflection of microwaves by a fast optically-controlled time-boundary. *Nat. Commun.* **15**, 6786 (2024).
- [38] Ren, Y. *et al.* Observation of momentum-gap topology of light at temporal interfaces in a time-synthetic lattice. *Nat. Commun.* **16**, 707 (2025).
- [39] Sharabi, Y., Lustig, E. & Segev, M. Disordered photonic time crystals. *Phys. Rev. Lett.* **126**, 163902 (2021).
- [40] Carminati, R., Chen, H., Pierrat, R. & Shapiro, B. Universal statistics of waves in a random time-varying medium. *Phys. Rev. Lett.* **127**, 094101 (2021).
- [41] Apffel, B., Wildeman, S., Eddi, A. & Fort, E. Experimental implementation of wave propagation in disordered time-varying media. *Phys. Rev. Lett.* **128**, 094503 (2022).
- [42] Garnier, J. Wave propagation in periodic and random time-dependent media. *Multiscale Model. Simul.* **19**, 1190–1211 (2021).
- [43] Kim, J., Lee, D., Yu, S. & Park, N. Unidirectional scattering with spatial homogeneity using correlated photonic time disorder. *Nat. Phys.* **19**, 726–732 (2023).

- [44] Eswaran, K. S., Kopaei, A. E. & Sacha, K. Anderson localization in photonic time crystals. *Phys. Rev. B* **111**, L180201 (2025).
- [45] Anderson, P. W. Absence of diffusion in certain random lattices. *Phys. Rev.* **109**, 1492–1505 (1958).
- [46] Gredeskul, S. A. *et al.* Anderson localization in metamaterials and other complex media. *Low Temp. Phys.* **38**, 570–602 (2012).
- [47] Sheinfux, H. H. *et al.* Observation of Anderson localization in disordered nanophotonic structures. *Science* **356**, 953–956 (2017).
- [48] Reck, P., Gorini, C., Goussev, A., Krueckl, V., Fink, M. & Richter, K. Dirac quantum time mirror. *Phys. Rev. B* **95**, 165421 (2017).
- [49] Junk, V., Reck, P., Gorini, C. & Richter, K. Floquet oscillations in periodically driven Dirac systems. *Phys. Rev. B* **101**, 134302 (2020).
- [50] Kim, S. & Kim, K. Propagation of Dirac waves through various temporal interfaces, slabs, and crystals. *Phys. Rev. Res.* **5**, 023162 (2023).
- [51] Ok, F., Bahrami, A. & Caloz, C. Electron scattering at a potential temporal step discontinuity. *Sci. Rep.* **14**, 5559 (2024).
- [52] Kim, S. & Kim, K. Spatial localization and diffusion of Dirac particles and waves induced by random temporal medium variations. *Commun. Phys.* **8**, 32 (2025).
- [53] Sipe, J. E., Sheng, P., White, B. S. & Cohen, M. H. Brewster anomalies: a polarization-induced delocalization effect. *Phys. Rev. Lett.* **60**, 108–111 (1988).
- [54] Lee, K. J. & Kim, K. Universal shift of the Brewster angle and disorder-enhanced delocalization of p waves in stratified random media. *Opt. Express* **19**, 20817–20826 (2011).
- [55] Kim, K. & Kim, S. Anderson localization and Brewster anomaly of electromagnetic waves in randomly-stratified anisotropic media. *Mater. Res. Express* **6**, 085803 (2019).
- [56] Kim, S. & Kim, K. Invariant imbedding theory of wave propagation in arbitrarily inhomogeneous stratified biisotropic media. *J. Opt.* **18**, 065605 (2016).
- [57] Kim, S. & Kim, K. Giant overreflection of magnetohydrodynamic waves from inhomogeneous plasmas with nonuniform shear flows. *Phys. Fluids* **34**, 127108 (2022).
- [58] Furutsu, K. On the statistical theory of electromagnetic waves in a fluctuating medium (I). *J. Res. Nat. Bur. Standards D* **67**, 303–323 (1963).



- [59] Novikov, E. A. Functionals and the random-force method in turbulence theory. *Sov. Phys. JETP* **20**, 1290–1294 (1965).
- [60] Mendonça, J. T. Temporal Klein model for particle-pair creation. *Symmetry* **13**, 1361 (2021).
- [61] Mei, J., Wu, Y., Chan, C. T. & Zhang, Z.-Q. First principles study of Dirac and Dirac-like cones in phononic and photonic crystals. *Phys. Rev. B* **86**, 035141 (2012).
- [62] Chan, C. T., Hang, Z. H. & Huang, X. Q. Dirac dispersion in two dimensional photonic crystals. *Adv. Optoelectron.* **2012**, 313984 (2012).
- [63] Castro Neto, A. H., Guinea, F., Peres, N. M. R., Novoselov, K. S. & Geim, A. K. The electronic properties of graphene. *Rev. Mod. Phys.* **81**, 109–162 (2009).
- [64] Peres, N. M. R. The transport properties of graphene: An introduction. *Rev. Mod. Phys.* **82**, 2673–2700 (2010).
- [65] Lherbier, A. Transport properties of graphene containing structural defects. *Phys. Rev. B* **86**, 075402 (2012).
- [66] Galiffi, E., Solís, D. M., Yin, S., Engheta, N. & Alù, A. Electrodynamics of photonic temporal interfaces. arXiv:2411.15984 [physics.optics].